Communication

Enhanced Deep Learning Approach Based on the Conditional Generative Adversarial Network for Electromagnetic Inverse Scattering Problems

He Ming Yao, Lijun Jiang, and Michael Ng

***Abstract*— This communication proposes a novel deep-learning (DL) framework for the electromagnetic inverse scattering (EMIS) problems. Solving EMIS problems is a challenging topic due to various difficulties, such as intrinsic nonlinearity, high computation cost, high contrast, and so on. To overcome these challenges, a novel DL-inspired approach is presented in the context of conditional deep convolutional generative adversarial network (CDCGAN), termed CDCGAN-EMIS. The proposed CDCGAN is based on a generator with an EM forward solver and the corresponding discriminator, both constructed by deep convolutional neural networks (DConvNets). During the offline training step, the generator learns a distribution between the measured scattered field data and the corresponding contrasts (permittivities) of dielectric scatterers, while the discriminator determines whether the presented samples are real or fake. Therefore, such CDCGAN-EMIS can generate contrasts of scatterers from measured scattered field data, by learning the distribution between the known contrasts of scatterers and their corresponding field and generating solutions. Based on the proposed CDCGAN-EMIS, EMIS problems can be accurately solved even for extremely high-contrast scatterers. Numerical examples indicate the accuracy and feasibility of our method. The proposed CDCGAN-EMIS opens a novel path for the DL-inspired real-time quantitative microwave imaging method for high-contrast scatterers.**

***Index Terms*— Convolutional generative adversarial network, electromagnetic inverse scattering (EMIS), high-contrast scatterer.**

I. Introduction

The electromagnetic inverse scattering (EMIS) problem is extensively applied in various fields, such as subsurface sensing [1], microwave imaging [2], biomedical imaging [3], and so on. The target of EMIS is exploring parameters by using received EM information [4], [5], [6]. In the past few years, a large number of methods have been reported for solving the EMIS problems, such as the subspace optimization method [7], contrast source inversion method [8], [9], contrast-source extended Born method [10], and Born iterative method [11]. Unluckily, the inevitable ill-posedness and nonlinearity bring large limitations to these conventional methods [1], [2], [3], [12]. These conventional methods usually employ regularization containing prior information, so that EMIS problems can be stably solved and the nonuniqueness can be relieved [12]. However, expressing prior information in rigorous mathematical formulations is usually quite difficult, so that it can hardly be incorporated [12]. Besides, these conventional methods include gradient-based deterministic methods, such as conjugate gradient methods and Gauss–Newton methods [13]. Their general aim is iteratively minimizing the corresponding objective functions, where their partial derivatives are computed with respect to model parameters in each optimization iteration. Consequently, these gradient-based deterministic methods usually suffer from higher memory and larger computation costs caused by their iteration computation. Moreover, the optimization is probably trapped in the local minima, because the derivatives cannot distinguish the global property and the local one.

Machine learning (ML) [14], [15] is rapidly progressing in modern computational science, such as high-performance computing [16], [17], [18], remote sensing [19], [20], and field-circuit cosimulation [21], [22]. ML techniques have also been proposed for EMIS problems. [23], [24] have made use of the artificial neural network (ANN) to solve EMIS problems. Recently, works originating from deep learning (DL) are being reported for EMIS problems [25], [26], [27], [28]. While DL approaches could illustrate relatively satisfactory results, the current DL-based methods can be summarized into three major categories.

1) The end-to-end DL-based method, where various DL modes are directly utilized to replace conventional methods, such as iterative optimization methods. In [26], [27], the initial inputs of the DL method are obtained by conventional methods, for example, the back-propagation (BP) method [29]. In [25], the encoder–decoder structure based on the deep convolutional neural networks (DConvNets) is proposed to directly use the measured scattered fields data as the input to solve the EMIS problems.

2) The cascaded structure method, where more than one component based on DL with individual functions are cascaded together to solve the EMIS problem [28], [29]. In [28], the two-step method was first proposed to solve EMIS problems, where the first step based on DConvNets is used to produce the coarsely reconstructed results for high-contrast scatterers, and the second step based on the U-net [27], [28] is further utilized to improve the quality of 'images.' [30] then presented a dual-module model for EMIS problems, where the conventional ANN with two hidden layers is used in the first step, followed by the U-net to improve the image quality.

3) The supervised gradient method (SDM) [14], [15], which includes the offline training step and the online application step [31], [32]. In its offline step, the training data are created with prior information. In the online step, the contrasts of samples are reconstructed by iteration computation using the learned descent gradients [31], [32]. However, during both offline and online processes, SDM cannot avoid EM forward computation in each optimization iteration [32].

In this work, we propose a novel DL framework for EMIS by utilizing a conditional deep convolutional generative adversarial network (CDCGAN) [33], [34], [35], termed CDCGAN-EMIS. The proposed CDCGAN-EMIS consists of the generator (G), the discriminator (D), and the forward solver (S). The generator (G) makes use of measured scattering data to generate the contrast

Manuscript received 2 August 2021; revised 12 October 2022; accepted 13 November 2022. Date of publication 17 June 2024; date of current version 9 July 2024. This work was supported in part by the Major Research Project on Scientific Instrument Development, National Natural Science Foundation of China under Grant 42327901; in part by Hong Kong Research Grants Council (HKRGC) General Research Fund (GRF) 17201020 and 17300021, C7004-21GF, and Joint NSFC-RGC N-HKU76921; and in part by the Fellowship Award from the Research Grants Council of the Hong Kong Special Administrative Region, China, under Grant HKU PDFS2122-7S05. *(Corresponding author: Michael Ng.)*

He Ming Yao is with the Department of Automation, Tsinghua University, Beijing 100084, China (e-mail: yaohmhk@connect.hku.hk).

Lijun Jiang is with the Department of Electrical and Electronic Engineering, The University of Hong Kong, Hong Kong, China (e-mail: jianglj@hku.hk).

Michael Ng is with the Department of Mathematics, Hong Kong Baptist University, Hong Kong, China (e-mail: michael-ng@hkbu.edu.hk).

Color versions of one or more figures in this article are available at https://doi.org/10.1109/TAP.2024.3388205.

Digital Object Identifier 10.1109/TAP.2024.3388205

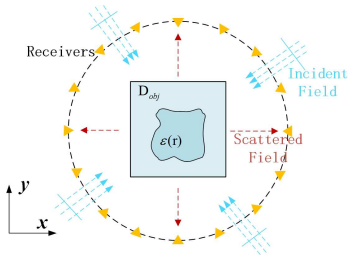

Fig. 1. Schematic of TM_z wave scattering in D_{obj}.

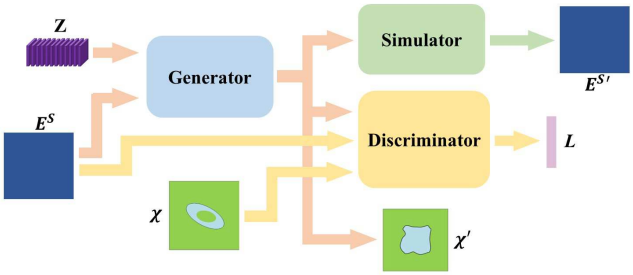

Fig. 2. Workflow of the proposed CDCGAN-EMIS: generator, Forward Solver, and discriminator constitute the complete architecture.

(permittivity) "images" of scatterers, while the discriminator (D) discriminates whether the generated "images" are real or fake. Plus, the Forward Solver (S) realizes the EM forward process and computes the EM scattered field resulting from the scatterers 'generated' from G, so that the performance of G can be further improved. The EM Forward Solver is based on the popular EM algorithm to realize EM forward computation, described in Section II. The advantages of this new DL framework can be summarized as: 1) during the offline training process, specific prior information can be employed to create training data. Thus, more prior information can flexibly be integrated to enhance this proposed DL method; 2) the usage of DConvNet greatly decreases the computation complexity of this DL-based method. Besides, as a typical learning-based method [25], [26], [27], [28], the proposed DL method only needs one-time computation and never requires iteration optimization, which is superior to conventional iterative optimization methods [1], [2], [3] and learning-based iterative methods [31], [32]. Therefore, it can realize real-time microwave imaging; and 3) the accuracy of this DL approach is better than traditional methods for solving EMIS problems.

II. Theory and Formulation

A. Problem Formulation

The schematic of EMIS is shown in Fig. 1, in which the objective domain (D_{obj}) is enveloped by M receivers uniformly distributed in space. While the TM_z incident field E^{in} illuminates D_{obj}, it is uniformly discretized into $N \times N$ pieces. M receivers work to receive EM scattered field E^s. Lippmann–Schwinger equations [36] formulate the whole EMIS process. The first formula is about interaction within EM field on fragments of D_{obj}.

$$E^t(\boldsymbol{r}) = E^{in}(\boldsymbol{r}) + k_0^2 \int_{D_{obj}} G(\boldsymbol{r},\boldsymbol{r}')\,\chi(\boldsymbol{r}')\,E^t(\boldsymbol{r}')\,d\boldsymbol{r}' \quad (1)$$

where the Green's function for 2-D TM_z wave is $G(\boldsymbol{r},\boldsymbol{r}') = -(j/4)H_0^{(2)}(k_0|\boldsymbol{r}-\boldsymbol{r}'|)$, where the second kind of zeroth-order Hankel function $H_0^{(2)}$ is utilized. $\boldsymbol{r}' = (x', y')$ and $\boldsymbol{r} = (x, y)$, respectively, represent the coordinates of the source and field points in D_{obj}. While k_0 is the wavenumber of free space and E^t is denoted as the total EM field. We also have $\chi(\boldsymbol{r}') = \varepsilon_r(\boldsymbol{r}') - 1$ as contrast function. The reradiation of the total field E^t of scatterers can be computed into the scattered field, the relationship of which is:

$$E^s(\boldsymbol{r}) = k_0^2 \int_{D_{obj}} G(\boldsymbol{r},\boldsymbol{r}')\,\chi(\boldsymbol{r}')\,E^t(\boldsymbol{r}')\,d\boldsymbol{r}' \quad (2)$$

where $\boldsymbol{r} = (x_R, y_R)$ denotes the position of receivers in D_{obj}. Solving EMIS problems has the aim of reconstructing the contrast χ (or permittivity ε_r) by EM scattered field. Usually, the traditional methods have to introduce the objective function $f(\chi)$, and try to reconstruct the contrast by optimization methods [6], shown in the following equation:

$$\min: f(\chi) = \sum_{i=1}^{N_i} \left\| E_i^s - E_i^s(\chi)' \right\| + \alpha T(\chi) \quad (3)$$

where N_i separate incident fields E^{in} of D_{obj} induce scattered fields E_i^s. During iterative optimization, $E_i^s(\chi)'$ gradually approaches E_i^s.

The traditional methods transform the (1) and (2) into the discretized form as [4], [6]

$$\bar{E}^s = \overline{\overline{G}}_R \cdot \mathrm{diag}\left(\bar{E}^t\right) \cdot \bar{\chi} \quad (4)$$

$$\bar{E}^t = \bar{E}^{in} + \overline{\overline{G}}_D \cdot diag\left(\bar{E}^t\right) \cdot \bar{\chi} \quad (5)$$

where the size of $\overline{\overline{G}}_R$ and $\overline{\overline{G}}_D$ can be set as $M \times N^2$ and $N^2 \times N^2$, respectively. Then, $\overline{\overline{G}}_R = k_0^2 S_{n'} G(\boldsymbol{r}_{n_r},\boldsymbol{r}_{n'})$ and $\overline{\overline{G}}_D = k_0^2 S_{n'} G(\boldsymbol{r}_n,\boldsymbol{r}_{n'})$, where $S_{n'}$ represents the area of the source piece, $n_r = 1, \ldots, M$, $n = 1, \ldots, N^2$, and $n' = 1, \ldots, N^2$.

B. CGAN Structure for EMIS

As the representative example of generative models, GANs model the training of a generative network as a two-player minimax game, where the generator is trained to learn a distribution of input and map to the generated images and balance its performance by the discriminator [33], [34], [35], [38]. CGAN develops the method to control the mapping from input to output by conditioning the standard generator and discriminator on 'extra information' (e.g., the difference between the 'generated' images and the ground-truthed images) [33], [34], [35]. Thanks to its flexibly-added 'extra information,' CGAN presents the superiority in image-based tasks [33], [34], [35].

In this communication, to realize reconstruction for high-contrast scatterers, CDCGAN-EMIS is proposed based on the discriminator and its corresponding generator with the Forward Solver for the EM forward process. In terms of difficulties in accumulating a large amount of training data in real experiments, the data from the simulation have been employed for training DL models. Unlike conventional GAN or CGAN models [33], [34], [35], [38], the proposed CDCGAN-EMIS never only aims at creating new contrast images. Instead, the proposed CDCGAN-EMIS is designed to learn the nonlinear mapping between the data distribution of scattered EM fields and the data distribution of the corresponding contrasts (permittivities) of the objective domain and further solve EMIS problems for the high-contrast samples with high precision. This proposed CDCGAN-EMIS considers both the difference between 'generated' contrast images and the ground-truthed contrast images, and the difference between the scattered field resulting from 'generated' contrast images and the input scattered field. In this way, the quality of reconstructed contrast images can be ensured with high accuracy.

As presented in Fig. 2, the proposed CDCGAN-EMIS consists of three modules: the generator (G), the discriminator (D), and the Forward Solver (S). The generator (G) makes use of measured scattered data to generate the contrast (permittivity) "images" of scatterers, while the discriminator (D) discriminates whether the generated "images" are real or fake. While G creates the scatterer 'images' according to its input EM scattered field E^s, the discriminator accepts both the ground-truthed scatterers 'images' and the 'images' generated from the generator and computes the

difference between the distributions of the two sets of data [33], [34], [35]. Thus, the discriminator guides the generator to create patterns that share common features with the input scatterers. As a typical CGAN structure, the difference between the created 'images' and the ground-truthed 'images' is taken into consideration to improve the performance of the prediction of G. Meanwhile, to make the structures 'learn' the effect of created scatterers on EM scattered field, the loss function also involves the difference between the input EM scattered field E^s from the generator and the EM scattered field E^s computed from the forward solver. During the training process, we update the weights in the generator by backpropagation from the losses defined by S and D.

1) The Forward Solver (S): The Forward Solver realizes the EM forward process, which computes the EM scattered field from targets. It is built to control the accuracy of the scattered EM field of the generated contrast images during the process of training the Generator. The popular method of moments (MoMs) is chosen to be implemented into this solver to realize the EM forward process [41], which does not require training and is also shown in (2). The selected method, that is, MoM, for the forward solver can ensure the accuracy of prediction for the trained models. Due to the forward solver, CDCGAN-EMIS can consider the difference between the scattered field resulting from 'generated' contrast images and the input scattered field. This difference will be added to the final loss of the generator. Thus, the quality of reconstructed contrast images can be evaluated from the perspective of their induced EM scattered fields. The details of the Forward Solver are also demonstrated in Fig. 2. Because of this EM Forward Solver, CDCGAN-EMIS can make use of both the EM inverse process and the EM forward process to evaluate the 'quality' of prediction, which is impossible for the black-box method [17], [25]. Moreover, because of this new evaluation mechanism, CDCGAN-EMIS can make use of all possible data to improve its understanding of EM's physical mechanism.
2) The Discriminator (D): The discriminator is based on the pixel-to-pixel DConvNet [14], [15], followed by the final classification layer [33], [34], [35], [38] to discriminate the realness of the 'images.' The detailed structure of the discriminator has been demonstrated in Fig. 3. Its input is the 'generated' target 'images' from the generator and the ground-truthed 'images,' both of which are with the size of $N \times N \times 2$ comprised of real and imaginary parts of contrast 'images.' Meanwhile, the final output discriminates the realness of the 'images.' Specifically, the discriminator repetitively makes use of 3×3 convolution with its stride as 2, leaky rectified linear unit (LeReLU), and batch normalization (BN). Besides, the 0.2 dropout operation is used [42].

The specific computation process is described by (6)

$$V(D,G) = E_{\chi\sim p_{\text{data}(\chi)}}\left[\log D\left(E^s,\chi\right)\right] + E_{(E^s,Z)\sim p_{(E^s,Z)}}\left[1-\log D\left(E^s,G\left(E^s,Z\right)\right)\right] \quad (6)$$

where Z represents the projected noise to the generator, while (E^s, Z) has been combined to be the condition data input to the generator. The noise Z is provided to the generator and defines what a generative sample is according to its distribution [38], [39], [40]. Additionally, $D()$ stands for the probability computed from the training dataset. While $G(E^s, Z)$ creates new contrast 'images', $D(E^s, G(E^s, Z))$ offers the probability of these generated 'images.' Based on these functions, all weights in the generator and discriminator will be updated iteratively. The aim of the training process is: 1) maximizing the probability of accuracy in discriminating samples created by the generator and that in training data and 2) minimizing $\log D(E^s, G(E^s, Z))$ to train the generator.

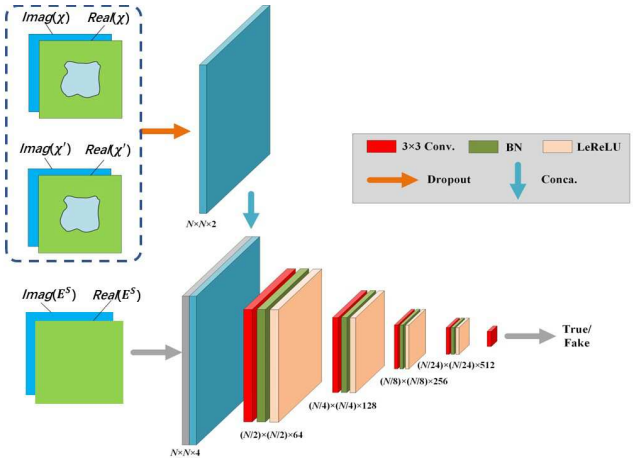

Fig. 3. Architecture of the discriminator for CDCGAN-EMIS.

1) The Generator (G): The generator of the proposed CDCGAN-EMIS originates from the deep convolutional encoder–decoder structure, which makes use of DConvNet and has demonstrated excellent performance for EMIS problems [25]. This structure is revised based on SegNet [43], which is extensively applied in the image segmentation field. The operation of the generator could be concluded to be the "heterogeneous" process, which transforms measured scattered fields into contrast 'images.' The objective of the generator is to generate data that the discriminator classifies as "real" [33], [34], [35], [38]. Thanks to the balancing operation of the discriminator, the generator can reasonably retrieve the contrast of scatterers from the scattered fields.

Fig. 4 shows the specific internal structure of the generator. Named as 'field data,' its input is set as the scattered field E^s, of which the size is $M \times N_i \times 2$. While N_i incident fields and M receivers interact in D_{obj}, the two tubes of input are filled by the real and imaginary parts of E^s. Meanwhile, the real and imaginary parts of scatterers are filled into the two tubes of output. The proposed model does not make use of the incidence E^{in}, because E^{in} keeps consistent for all tests and there are no specific features for the proposed method.

In Fig. 4, three important parts are combined together into our designed generator: encoding, decoding, and projecting. While its encoding part encodes 'field image' E^s and refines the input into chunks of feature fragments, its decoding counterpart reinstalls the feature fragments to generate the predicted contrast χ'. The middle projecting part projects and reshapes the noise input Z into the structure to upscale the noise Z using a fully connected operation and reshapes the output to the specified size. Specifically speaking, the encoding part comprises the reduplicated usage of convolution with the stride as 2, ReLU, and BN. Comparatively, the following decoding part involves reduplicated usage of operations of up-convolution with its stride as 2, BN, and ReLU, followed by the final convolution layer, while a hyperbolic tangent (tanh) activation layer is installed to the end, as shown in Fig. 4.

$$\chi' = G\left(E^s, Z\right). \quad (7)$$

The whole process in the generator is concluded as a 'heterogeneous' process, shown in (7), where the received scattered EM field is transformed into the contrast 'images' of scatterers. In this process, the deep convolutional encoder–decoder architecture transfer E^s and Z into the final output χ. Hence, the generator can entirely complete all operations of the traditional methods [7], [8], [9], [10], [11].

We should highligh some issues related to the generator model.

1) Loss Function: While the loss function directly decides the objective and the physical meaning of the generator, we have

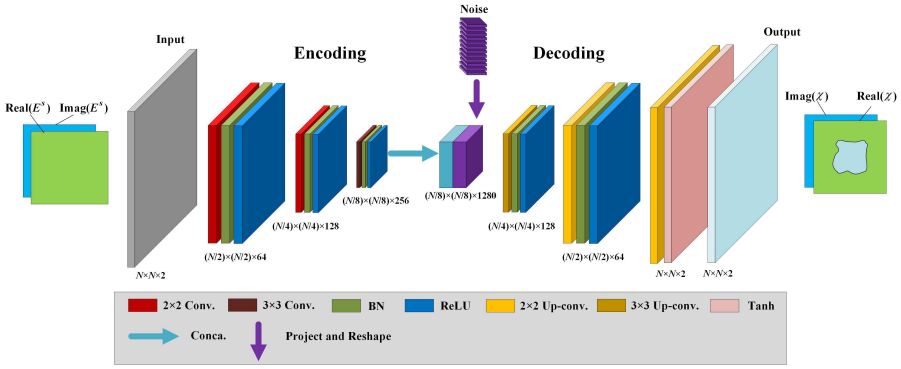

Fig. 4. Architecture of the generator for CDCGAN-EMIS.

to simultaneously take balance and difference into consideration. We revised the loss function of the conventional CGAN by adding L_S, shown in (8) and (9). In fact, the conventional CGAN usually uses the first two terms (i.e., L_G and L_p) in (8) as the loss function [33], [34], [35], because conventional image problems are not involved in the physical meaning of EM scattering. In other words, we here add the error between E^s and $E^{s\prime}$ into the loss function to estimate the effect of the 'image' error on the EM scattering, shown in (9). In this way, both the quality of the predicted 'EM image' and its effect on EM scattering can be taken into consideration.

Thus, the full loss function of the generator is denoted as the following equations:

$$L_F = L_G + \lambda_1 L_p + \lambda_2 L_S \tag{8}$$

$$L_S = \frac{1}{N}\|E^s - E^{s\prime}\|^2 \tag{9}$$

$$L_p = \frac{1}{N}\|\chi - \chi'\|^2 \tag{10}$$

where L_G denotes the adversarial loss derived from (6). While L_p indicates the mean square error (MSE) between χ and the generated χ', L_S estimates the difference between E^s and $E^{s\prime}$, shown in (9) and (10). While $\lambda_1 = 50$ and $\lambda_2 = 100$ are denoted as the weighing parameters that represent the proportion of L_p and L_S that account for L_F and also demonstrate the importance of χ and E^s. As shown in (11), L_G represents the adversarial loss function for the generator, which has been usually used for the conventional CGAN [33], [34].

$$L_G = -\frac{1}{m}\sum_{i=1}^{m}\left[\log\left(1 - D\left(E^{s,i}, G\left(E^{s,i}, Z^i\right)\right)\right)\right] \tag{11}$$

where m stands for the batch size, while i is the ith data in the batch.

Meanwhile, the loss function of the discriminator is defined as

$$L_D = -\frac{1}{m}\sum_{i=1}^{m}\left[\log\left(D\left(E^{s,i}, G\left(E^{s,i}, Z^i\right)\right)\right)\right] - \frac{1}{m}\sum_{i=1}^{m}\left[\log\left(1 - D\left(E^{s,i}, \chi^i\right)\right)\right]. \tag{12}$$

During the training process, the discriminator tries to make the score of ground truth close to 1 and that of fake inputs close to 0 [33], [34], [35], [38].

2) Computational Complexity: The computation of the proposed generator is done on the reduplicated usage of convolutions, BN, and activation layers, where the operation count depends on convolution operation due to the small size of the filter kernel [25], [26], [27], [28], [44]. For its encoder part, the input has the size of $M \times N_i \times 2$, while R filters have the size of $K \times K$ in all f layers. Hence, its computation complexity is $O(MN_i\ K^2R^2F)$ [44]. Plus, the computation in the decoding part actually shares the same operation as the encoding part (in the opposite direction). Therefore, while they share the same scale of parameters, only their output size (as input in the encoding part) becomes $N \times N \times 2$. Hence, the computational complexity in the decoding part can be concluded as $O(N^2K^2R^2f)$. Usually, the size of input field "image" is chosen to be approximated to that of the output contrast "image" [25], [26], [27]. Thus, the generator approximately has the computational complexity of $O(N^2f^2R^2f)$ [44], which is smaller than most of conventional iterative optimization methods for EMIS, including Gauss–Newton [1], [2], [3], and the iterative learning-based method, such as SDM [31], [32].

III. Numerical Examples

A. Numerical Setup and Offline Training

In this section, the specific offline training and testing of CDCGAN-EMIS are described. It should be highlighted that the training of the proposed CDCGAN-EMIS is merely based on one group of synthetic datasets, that is, MNIST [25], [26], [27], [28]. In D_{obj} presented in Fig. 1, each sample from MNIST has the size as $\lambda \times \lambda$ ($\lambda = 1$ m is the wavelength in free space) with the relative permittivity ε_r, while each sample is evenly discretized as 20×20 fragments (i.e., N 20). D_{obj} is uniformly surrounded by 20 receivers ($M = 20$) with the distance as 30 λ, while 20 TM_z incident plane waves, respectively, illuminate D_{obj} from the direction evenly distributed within [0°, 360°), (i.e., $N_i = 20$). The training and testing data are created by the full-wave EM simulations [45]. As the challenge for the traditional methods, we set the relative permittivity of the non-homogeneous number-shaped scatterers from MNIST as $\varepsilon_r \in (1, 8]$. We randomly choose 5000 samples from MNIST to create the training data. Normalized mean-square error (NMSE) and structural similarity index (SSIM) have been used as quantitative indicators to explain the result of retrieved "images" [25], [26], [27]. For comparison, the Gauss–Newton method [13] has been employed to reconstruct the contrasts of the samples, as illustrated in Sections III-B and III-C.

In fact, training GANs is challenging, because the generator and the discriminator compete against each other during the training. Usually, if one network learns too quickly, the other network may fail to learn [38]. The training in this work involves the training of both discriminator and generator with the alternating order method [33], [34], [35], [38]. We highlight that the discriminator has to take the 'frozen' operation, which means it will not be trainable. In this way, during the process of training the generator, the weights of the discriminator are not to be updated. This newly proposed CDCGAN-EMIS is benchmarked in MATLAB 2020a with DL Toolbox [46]. Adaptive Moment Estimation (Adam) optimizer is utilized to optimize the loss function.

B. Performance on Number-Shaped Scatterers

In Section II-B, the proposed CDCGAN-EMIS has been tested on 1000 new samples from MNIST. Fig. 5 presents the comparison between the reconstruction from the Gauss–Newton method and that from this DL method (the imaginary part of the contrast of scatterers is all zero, and the corresponding channels are all zero).

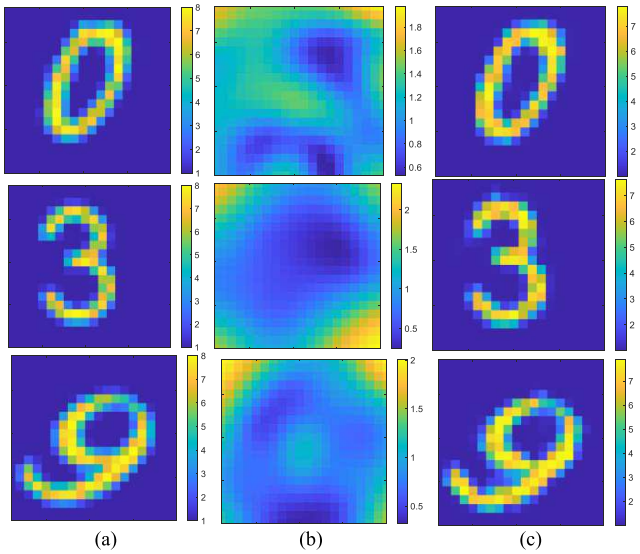

(a) (b) (c)

Fig. 5. Comparisons of retrieved relative permittivities of scatterers in MNIST. (a) Ground truth. (b) Gauss–Newton. (c) CDCGAN-EMIS.

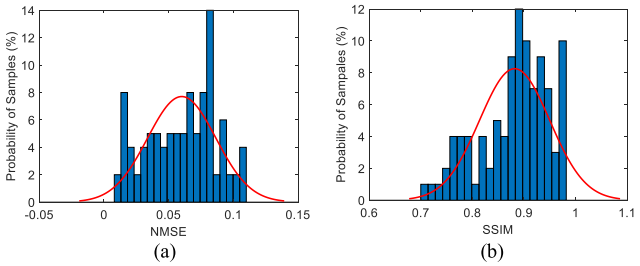

(a) (b)

Fig. 6. Performance of the proposed CDCGAN-EMIS on the MNIST dataset: Statistical histograms of the image quality for the retrieved permittivities and fitting of its normal density function. (a) NMSE. (b) SSIM.

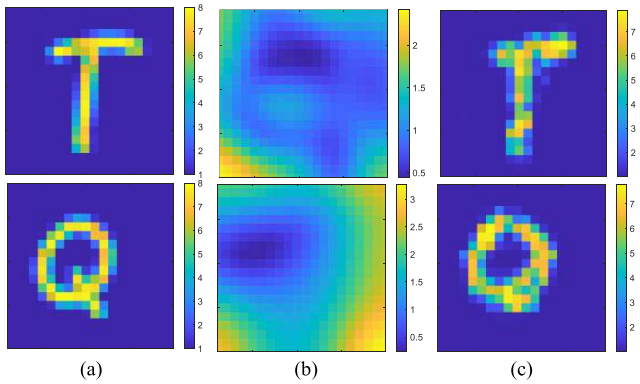

(a) (b) (c)

Fig. 7. Comparisons of retrieved relative permittivities of scatterers in 'Letter'. (a) Ground truth. (b) Gauss–Newton. (c) CDCGAN-EMIS.

So, we do not present the image for this channel. Besides, in Sections III-B and III-C, the image for the all-zero channel will also not be presented. Obviously, the final outputs match much well with their corresponding ground truth, despite the new sample shape and extremely high heterogeneous contrast. But, the traditional method (Gauss–Newton method) nearly cannot realize successful reconstruction. What is more, as shown in Table I, this proposed DL approach needs less time to complete a computation than the Gauss–Newton approach. Actually, the Gauss–Newton method has to use about 6 s to complete 10× iteration computation for one test sample, while the final reconstruction results are very bad, as presented in Fig. 5. On the contrary, this proposed CDCGAN-EMIS merely uses less than 0.03 s to successfully realize reconstruction for one sample with high precision. In addition, this CDCGAN-EMIS only requires one-time computation and never needs iteration computation.

TABLE I

PERFORMANCE COMPARISON OF CDCGAN-EMIS AND GAUSS–NEWTON

Reconstruction	MNIST	Letter
CDCGAN-EMIS	0.029028s	0.028924s
Gauss-Newton (10 times iteration)	5.95312s	6.01896s

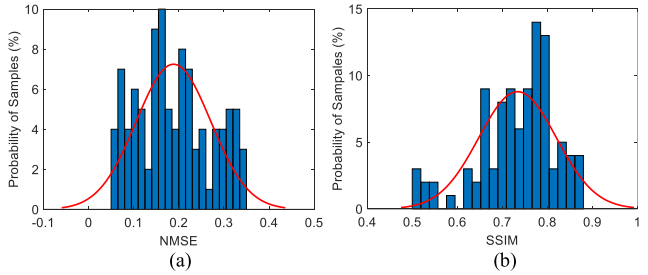

(a) (b)

Fig. 8. Performance of the proposed CDCGAN-EMIS on 'Letter' datasets: Statistical histograms of the image quality for the retrieved permittivities and fitting of its normal density function. (a) NMSE. (b) SSIM.

In Fig. 6, the statistical analysis of tests is demonstrated: NMSE of reconstruction obtained from the generator has the average as about 0.05, while the SSIM average obtained from this proposed method could overcome 0.9. Hence, EMIS problems could be successfully solved by our CDCGAN-EMIS.

C. Performance on Letter-Shaped Scatterers

In this section, a new synthetic dataset, called 'Letter,' is proposed to demonstrate the power and generality of the proposed CDCGAN-EMIS. In 'Letter', the nonhomogeneous letter-shaped scatterers are assumed to be randomly located in D_{obj}. The size of samples in 'Letter' has been set to $\lambda \times \lambda$, while their relative permittivities ε_r are randomly set into the range of (1,8].

Fig. 7 illustrates the comparison between the reconstruction from the Gauss–Newton approach and that from our proposed CDCGAN-EMIS. Similarly, its final reconstruction outputs match much well with the ground truth, despite the extremely high heterogeneous contrast and the new test sample shapes. However, Gauss–Newton nearly cannot realize successful reconstruction. What is more, as shown in Table I, this proposed approach uses less time (less than 0.03 s) to complete a computation than the Gauss–Newton method. Taking into consideration that the training of this DL model merely relies on MNIST, its final predictions for 'Letter' can demonstrate its success in realizing EM inversion. These results also have illustrated the excellent generalization ability of this CDCGAN-EMIS. We randomly select 1000 samples from 'Letter' to evaluate the reconstruction performance of CDCGAN-EMIS. Fig. 8 presents the statistical analysis for reconstruction performance on the selected samples NMSE average of retrieved results of the generator arrives at about 0.2, while the SSIM average of the generator could overcome 0.74, which shows CDCGAN-EMIS can successfully solve EMIS problems.

IV. CONCLUSION

The new DL framework for EMIS problems has been proposed, based on CDCGAN. The proposed CDCGAN-EMIS can solve various challengeable EMIS problems for conventional methods, such as high contrast, intrinsic nonlinearity, high computation cost, and so on. The proposed CDCGAN is based on the generator with an EM Forward Solver and the corresponding discriminator. In the offline training of the proposed CDCGAN-EMIS, the generator learns 'mapping' between the scattered field data and the corresponding contrasts of dielectric scatterers, while the discriminator evaluates the presented samples. As a result, the proposed CDCGAN-EMIS can

generate contrasts of scatterers from measured scattered field data, by "learning" mapping between the known contrasts of scatterers and their corresponding field and "composing" new solutions. Based on the proposed CDCGAN-EMIS, EMIS problems can be accurately solved even in extremely high-contrast scatterers cases. Numerical examples demonstrate its feasibility and precision. The proposed CDCGAN-EMIS provides novel thinking for DL-inspired real-time quantitative microwave imaging methods for high-contrast scatterers.

REFERENCES

[1] W. C. Chew et al., "Nonlinear diffraction tomography: The use of inverse scattering for imaging," *Int. J. Imag. Syst. Technol.*, vol. 7, no. 1, pp. 16–24, 1996.

[2] A. Abubakar, T. M. Habashy, G. Pan, and M.-K. Li, "Application of the multiplicative regularized Gauss–Newton algorithm for three-dimensional microwave imaging," *IEEE Trans. Antennas Propag.*, vol. 60, no. 5, pp. 2431–2441, May 2012.

[3] J. Behura, K. Wapenaar, and R. Snieder, "Autofocus imaging: Image reconstruction based on inverse scattering theory," *Geophysics*, vol. 79, no. 3, pp. 19–26, May 2014.

[4] M. Pastorino, *Microwave Imaging*. Hoboken, NJ, USA: Wiley, 2010.

[5] P. M. Meaney, M. W. Fanning, D. Li, S. P. Poplack, and K. D. Paulsen, "A clinical prototype for active microwave imaging of the breast," *IEEE Trans. Microw. Theory Techn.*, vol. 48, no. 11, pp. 1841–1853, Nov. 2000.

[6] M. Li and A. Abubakar, "Electromagnetic inverse problems [guest editorial]," *IEEE Antennas Propag. Mag.*, vol. 59, no. 5, pp. 9–115, Oct. 2017.

[7] Y. Liu, Z. Zhao, X. Zhu, Z. Nie, and Q. H. Liu, "A CSEB subspace-based optimization method for reconstruction of uniaxial anisotropic objects," in *Proc. Prog. Electromagn. Res. Symp.*, Nov. 2017, pp. 93–98.

[8] A. Abubakar and P. M. V. D. Berg, "The contrast source inversion method for location and shape reconstructions," *Inverse Problems*, vol. 18, no. 2, pp. 495–510, Apr. 2002.

[9] M. Li, O. Semerci, and A. Abubakar, "A contrast source inversion method in the wavelet domain," *Inverse Problems*, vol. 29, no. 2, Feb. 2013, Art. no. 025015.

[10] L. Crocco, M. D'Urso, and T. Isernia, "Testing the contrast source extended born inversion method against real data: The TM case," *Inverse Problems*, vol. 21, no. 6, pp. 33–50, Dec. 2005.

[11] M. Moghaddam and W. C. Chew, "Study of some practical issues in inversion with the Born iterative method using time-domain data," *IEEE Trans. Antennas Propag.*, vol. 41, no. 2, pp. 177–184, Feb. 1993.

[12] K. I. Hopcraft and P. R. Smith, *An Introduction to Electromagnetic Inverse Scattering*. Boston, MA, USA: Kluwer, 1992.

[13] X. Xiong and F. de la Torre, "Supervised descent method and its applications to face alignment," in *Proc. IEEE Conf. Comput. Vis. Pattern Recognit.*, Jun. 2013, pp. 532–539.

[14] Y. LeCun, Y. Bengio, and G. Hinton, "Deep learning," *Nature*, vol. 521, no. 7553, pp. 436–444, 2015.

[15] C. M. Bishop, *Pattern Recognition and Machine Learning*. Berlin, Germany: Springer-Verlag, 2006.

[16] H. M. Yao and L. Jiang, "Machine-learning-based PML for the FDTD method," *IEEE Antennas Wireless Propag. Lett.*, vol. 18, no. 1, pp. 192–196, Jan. 2019.

[17] H. H. Zhang, H. M. Yao, L. Jiang, and M. Ng, "Deep long-short term memory networks based solving method for the FDTD method: 2D case," *IEEE Microw. Wireless Compon. Lett.*, vol. 33, no. 5, pp. 499–502, May 2023.

[18] H. M. Yao, L. Jiang, and M. Ng, "Implementing the fast full-wave electromagnetic forward solver using the deep convolutional encoder–decoder architecture," *IEEE Trans. Antennas Propag.*, vol. 71, no. 1, pp. 1152–1157, Jan. 2023.

[19] R. Guo, H. M. Yao, M. Li, M. K. P. Ng, L. Jiang, and A. Abubakar, "Joint inversion of audio-magnetotelluric and seismic travel time data with deep learning constraint," *IEEE Trans. Geosci. Remote Sens.*, vol. 59, no. 9, pp. 7982–7995, Sep. 2021.

[20] S. Chen, H. Wang, F. Xu, and Y.-Q. Jin, "Target classification using the deep convolutional networks for SAR images," *IEEE Trans. Geosci. Remote Sens.*, vol. 54, no. 8, pp. 4806–4817, Aug. 2016.

[21] H. H. Zhang, L. J. Jiang, and H. M. Yao, "Embedding the behavior macromodel into TDIE for transient field-circuit simulations," *IEEE Trans. Antennas Propag.*, vol. 64, no. 7, pp. 3233–3238, Jul. 2016.

[22] H. H. Zhang, L. J. Jiang, H. M. Yao, and Y. Zhang, "Transient heterogeneous electromagnetic simulation with DGTD and behavioral macromodel," *IEEE Trans. Electromagn. Compat.*, vol. 59, no. 4, pp. 1152–1160, Aug. 2017.

[23] S. Caorsi and P. Gamba, "Electromagnetic detection of dielectric cylinders by a neural network approach," *IEEE Trans. Geosci. Remote Sens.*, vol. 37, no. 2, pp. 820–827, Mar. 1999.

[24] I. T. Rekanos, "Inverse scattering of dielectric cylinders by using radial basis function neural networks," *Radio Sci.*, vol. 36, no. 5, pp. 841–849, Sep. 2001.

[25] H. M. Yao, L. Jiang, and W. E. I. Sha, "Enhanced deep learning approach based on the deep convolutional encoder–decoder architecture for electromagnetic inverse scattering problems," *IEEE Antennas Wireless Propag. Lett.*, vol. 19, no. 7, pp. 1211–1215, Jul. 2020.

[26] L. Li, L. G. Wang, F. L. Teixeira, C. Liu, A. Nehorai, and T. J. Cui, "DeepNIS: Deep neural network for nonlinear electromagnetic inverse scattering," *IEEE Trans. Antennas Propag.*, vol. 67, no. 3, pp. 1819–1825, Mar. 2019.

[27] L. Li, L. G. Wang, and F. L. Teixeira, "Performance analysis and dynamic evolution of deep convolutional neural network for electromagnetic inverse scattering," *IEEE Antennas Wireless Propag. Lett.*, vol. 18, pp. 2259–2263, 2019.

[28] H. M. Yao, W. E. I. Sha, and L. Jiang, "Two-step enhanced deep learning approach for electromagnetic inverse scattering problems," *IEEE Antennas Wireless Propag. Lett.*, vol. 18, pp. 2254–2258, 2019.

[29] K. Belkebir, P. C. Chaumet, and A. Sentenac, "Superresolution in total internal reflection tomography," *J. Opt. Soc. Amer. A, Opt. Image Sci.*, vol. 22, no. 9, pp. 1889–1897, 2005.

[30] L. Xiao, J. Li, F. Han, W. Shao, and Q. H. Liu, "Dual-module NMM-IEM machine learning for fast electromagnetic inversion of inhomogeneous scatterers with high contrasts and large electrical dimensions," *IEEE Trans. Antennas Propag.*, vol. 68, no. 8, pp. 6245–6255, Aug. 2020.

[31] H. M. Yao, R. Guo, M. Li, L. Jiang, and M. K. P. Ng, "Enhanced supervised descent learning technique for electromagnetic inverse scattering problems by the deep convolutional neural networks," *IEEE Trans. Antennas Propag.*, vol. 70, no. 8, pp. 6195–6206, Aug. 2022.

[32] R. Guo et al., "Pixel- and model-based microwave inversion with supervised descent method for dielectric targets," *IEEE Trans. Antennas Propag.*, vol. 68, no. 12, pp. 8114–8126, Dec. 2020.

[33] M. Mirza and S. Osindero, "Conditional generative adversarial nets," 2014, *arXiv:1411.1784*.

[34] P. Isola, J.-Y. Zhu, T. Zhou, and A. A. Efros, "Image-to-image translation with conditional adversarial networks," 2016, *arXiv:1611.07004*.

[35] G. Antipov, M. Baccouche, and J.-L. Dugelay, "Face aging with conditional generative adversarial networks," in *Proc. IEEE Int. Conf. Image Process. (ICIP)*, Sep. 2017, pp. 2089–2093.

[36] M. A. Fiddy and R. S. Ritter, *Introduction to Imaging From Scattered Fields*. Boca Raton, FL, USA: CRC Press, 2014.

[37] A. L. Da Cunha, J. Zhou, and M. N. Do, "The nonsubsampled contourlet transform: Theory, design, and applications," *IEEE Trans. Image Process.*, vol. 15, no. 10, pp. 3089–3101, Oct. 2006.

[38] I. Goodfellow et al., "Generative adversarial nets," in *Proc. Int. Conf. Neural Inf. Process. Syst.*, 2014, pp. 2672–2680.

[39] H. Zhang, V. Sindagi, and V. M. Patel, "Image de-raining using a conditional generative adversarial network," *IEEE Trans. Circuits Syst. Video Technol.*, vol. 30, no. 11, pp. 3943–3956, Nov. 2020.

[40] G. Yang et al., "DAGAN: Deep de-aliasing generative adversarial networks for fast compressed sensing MRI reconstruction," *IEEE Trans. Med. Imag.*, vol. 37, no. 6, pp. 1310–1321, Jun. 2018.

[41] R. F. Harrington, *Field Computation by Moment Methods*. Hoboken, NJ, USA: Wiley, 1993.

[42] N. Srivastava, G. Hinton, A. Krizhevsky, I. Sutskever, and R. Salakhutdinov, "Dropout: A simple way to prevent neural networks from overfitting," *J. Mach. Learn. Res.*, vol. 15, no. 1, pp. 1929–1958, 2014.

[43] V. Badrinarayanan, A. Kendall, and R. Cipolla, "SegNet: A deep convolutional encoder–decoder architecture for image segmentation," *IEEE Trans. Pattern Anal. Mach. Intell.*, vol. 39, no. 12, pp. 2481–2495, Dec. 2017.

[44] K. H. Jin, M. T. McCann, E. Froustey, and M. Unser, "Deep convolutional neural network for inverse problems in imaging," *IEEE Trans. Image Process.*, vol. 26, no. 9, pp. 4509–4522, Sep. 2017.

[45] M. F. Catedra, *The CG-FFT Method: Application of Signal Processing Techniques to Electromagnetics*. Boston, MA, USA: Artech House, 1995.

[46] P. Kim, *MATLAB Deep Learning*. New York, NY, USA: Apress, 2017.